# Stacking faults as quantum wells in nanowires: Density of states, oscillator strength, and radiative efficiency

P. Corfdir,* C. Hauswald, J. K. Zettler, T. Flissikowski, J. Lähnemann, S. Fernández-Garrido, L. Geelhaar, H. T. Grahn, and O. Brandt

*Paul-Drude-Institut für Festkörperelektronik, Hausvogteiplatz 5-7, 10117 Berlin, Germany*

(Received 19 August 2014; published 18 November 2014)

We investigate the nature of excitons bound to $I_1$ basal-plane stacking faults [$(I_1,X)$] in GaN nanowire ensembles by continuous-wave and time-resolved photoluminescence spectroscopy. Based on the linear increase of the radiative lifetime of these excitons with temperature, they are demonstrated to exhibit a two-dimensional density of states, i.e., a basal-plane stacking fault acts as a quantum well. From the slope of the linear increase, we determine the oscillator strength of the $(I_1,X)$ and show that the value obtained reflects the presence of large internal electrostatic fields across the stacking fault. While the recombination of donor-bound and free excitons in the GaN nanowire ensemble is dominated by nonradiative phenonema already at 10 K, we observe that the $(I_1,X)$ recombines purely radiatively up to 60 K. This finding provides important insight into the nonradiative recombination processes in GaN nanowires. First, the radiative lifetime of about 6 ns measured at 60 K sets an upper limit for the surface recombination velocity of 210 cm s$^{-1}$ considering the nanowires mean diameter of 50 nm. Second, the density of nonradiative centers responsible for the fast decay of donor-bound and free excitons cannot be higher than $6 \times 10^{16}$ cm$^{-3}$. As a consequence, the nonradiative decay of donor-bound excitons in these GaN nanowire ensembles has to occur indirectly via the free exciton state.

DOI: 10.1103/PhysRevB.90.195309 PACS number(s): 78.67.Uh, 71.35.−y, 71.55.Eq, 78.47.jd

## I. INTRODUCTION

One remarkable property of III-V semiconductor nanowires is their ability to adopt both the wurtzite or zinc-blende crystal structure [1]. This fact has opened the possibility to realize crystal-phase quantum structures, i.e., heterostructures in which confinement is achieved by alternation of the crystal structure of a given semiconductor [2–5]. The major attractions of crystal-phase quantum structures are the absence of strain and alloy disorder as well as the atomically abrupt interfaces between the constituent crystal phases [4,6], i.e., they are expected to possess an exceptionally high structural perfection. In fact, very narrow linewidths have been reported for the characteristic emission lines observed for these structures [4,7–9]. Consequently, crystal-phase quantum structures have been promoted as candidates for optoelectronic applications such as lasers or single-photon emitters [4,10,11]. Recent progress in the understanding of growth mechanisms has made it possible to grow nanowires with controlled crystal-phase superlattices [2,3] or nanowires with only a few crystal-phase quantum disks [4,12,13].

The prototypic crystal-phase quantum structure in a wurtzite crystal is the intrinsic $I_1$ basal-plane stacking fault (BSF). It has been proposed that the $I_1$ BSF may be considered to represent a three monolayer thick zinc-blende quantum well (QW) in a wurtzite matrix [14]. This assertion was supported theoretically by the *ab initio* calculations in Ref. [15]. A recent experimental report by Korona et al. [16] also suggested that $I_1$ BSFs in GaN can be considered as QWs. However, little is known about the nature of the excitons confined in these QWs. In particular, a quantitative knowledge of their oscillator strength and radiative efficiency would be essential for a qualified assessment of the actual potential of crystal-phase quantum structures for optoelectronic applications.

In this work, we investigate the dynamics of excitons bound to $I_1$ BSFs in GaN nanowire ensembles [$(I_1,X)$]. Based on the evolution of their radiative lifetime with temperature, we show unambiguously that the $(I_1,X)$ exhibit a two-dimensional density of states, and we determine their oscillator strength. Their decay is purely radiative up to 60 K, allowing us to estimate the maximum surface recombination velocity of the nanowires $M$-plane sidewalls as well as the maximum density of nonradiative centers in the nanowires. For higher temperatures, the radiative efficiency of the $(I_1,X)$ decreases as a result of their thermal escape from the BSFs.

## II. EXPERIMENT

The GaN nanowire ensemble studied here is formed spontaneously during plasma-assisted molecular beam epitaxy on a Si(111) substrate [17–19]. The nanowires are on the average 2 μm long and exhibit a mean diameter of 50 nm. The sample was prepared at high substrate temperature (875 °C) and a Ga/N flux ratio higher than one to compensate for the high Ga desorption rate at this temperature [20]. As a result of these conditions, we observe melt-back etching of the Si substrate arising from the formation of a Ga-Si eutectic alloy [21]. Photoluminescence (PL) experiments revealed that the melt-back etching of the Si substrate during the formation of the GaN nanowire ensemble leads to both unintentional Si doping and the formation of a high density of BSFs [21]. The latter phenomenon is rarely observed in GaN nanowires prepared using conventional growth conditions, i.e., substrate temperatures $\leqslant$820 °C and Ga/N flux ratios well below one [17,22]. More details about the substrate preparation and the specific growth conditions can be found elsewhere [21].

*corfdir@pdi-berlin.de

 

The present sample was chosen for its narrow near-band-edge and strong BSF emission at 10 K, both of which are characteristics for GaN nanowire ensembles grown above 850 °C [21]. However, the conclusions drawn in this article have been verified for several samples with very different morphologies and BSF densities (see Appendix B).

Continuous-wave (cw) PL experiments were carried out with a HeCd laser for excitation ($\lambda = 325$ nm). The laser beam with a power of less than 150 nW was focused onto the sample surface to a 1 μm diameter spot using a microscope objective with a numerical aperture of 0.65. The emitted light was collected using the same objective and then directed to a monochromator (focal length 80 cm, 600 lines per mm grating) followed by a charge-coupled device (CCD) camera. Time-resolved (TR) PL spectroscopy was performed using the second harmonic ($\lambda = 325$ nm) of fs pulses obtained from an optical parametric oscillator pumped by a Ti:sapphire laser with a repetition rate of 76 MHz. We used an energy fluence per pulse of 1 μJ cm$^{-2}$. The emitted light was dispersed using a monochromator with a 22 cm focal length and a 1800 lines per mm grating. The dispersed light was then directed to a streak camera that can be operated either in synchroscan or in single sweep mode. For both cw and TR PL, the samples were mounted on a coldfinger cryostat whose temperature $T$ was varied between 10 and 300 K. For the TR PL experiments, one expects a significant deviation between the lattice temperature and the effective temperature of the exciton gas. Consequently, throughout this paper, the temperature specified for TR PL experiments is the effective carrier temperature, which we extract from the PL spectra as detailed in Ref. [22]. Cathodoluminescence spectroscopy (CL) was performed in a scanning electron microscope with the acceleration voltage and probe current set to 3 kV and 500 pA, respectively. The emitted light was collected with a parabolic mirror, dispersed by a monochromator (focal length 30 cm, 1200 lines per mm grating) and detected by a photomultiplier.

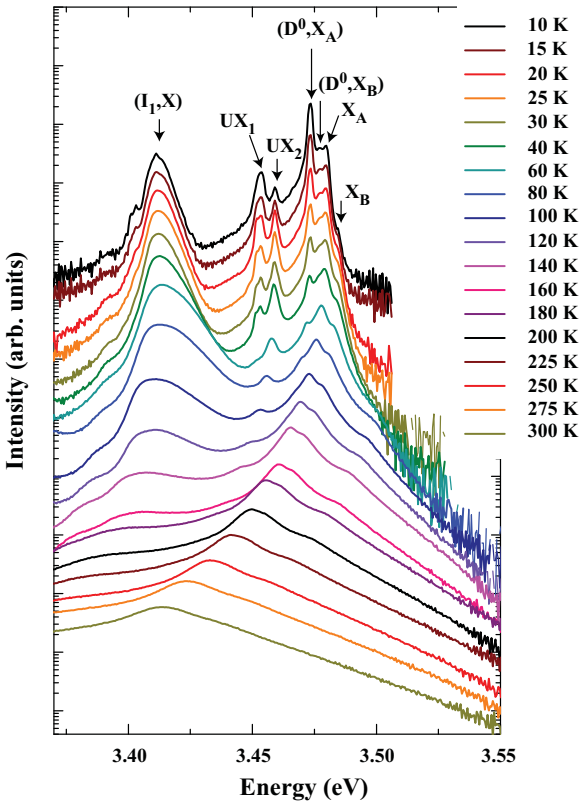


FIG. 1. (Color online) Continuous-wave PL spectra of the GaN nanowire ensemble under consideration for various temperatures as indicated in the figure. The spectra are shifted vertically for clarity. The major transitions are labeled according to their origin.

## III. RESULTS AND DISCUSSION

### A. Temperature-dependent spectra of the stacking-fault exciton

Figure 1 shows the PL spectra of the GaN nanowire ensemble under investigation at temperatures between 10 and 300 K. At 10 K, the spectrum is dominated by a strong line at 3.472 eV that originates from the recombination of A excitons bound to neutral donors [$(D^0,X_A)$]. We attribute the weaker line at 3.476 eV to the emission from donor-bound B excitons [$(D^0,X_B)$]. The emission from free A excitons ($X_A$) and free B excitons ($X_B$) are also resolved at 3.4785 and 3.484 eV, respectively. In this paper, we are not interested in the detailed interplay between $(D^0,X_A)$ and $(D^0,X_B)$. Therefore, in the following, the emission intensity spectrally integrated over the $(D^0,X_A)$ and $(D^0,X_B)$ lines is simply denoted as $(D^0,X)$. Similarly, from now on the emission integrated over the $X_A$ and $X_B$ lines is labeled FX. On the low energy side of the $(D^0,X)$ emission, we observe two bands centered at 3.452 and 3.458 eV labeled $UX_1$ and $UX_2$, respectively [23]. The origin of these bands has not been established beyond doubt, but we believe them to be related to the nanowire surface [22,24]. Note that these transitions are superimposed onto those associated with the two-electron satellites of the $(D^0,X)$ transitions from the core of the nanowires [22]. Finally, the broadband centered at 3.410 eV arises from the radiative decay of the $(I_1,X)$ [8,25–27]. We attribute the slight deviation of the $(I_1,X)$ transition energy from values reported for GaN layers [25–27] to variations in the local stacking fault density [28] and in the magnitude of the built-in electric fields along the $c$ axis [8,28].

Low-temperature CL maps taken at the $(D^0,X)$ and $(I_1,X)$ emission energies are displayed in Figs. 2(a) and 2(b), respectively. The $(D^0,X)$ transition is found to be much stronger in the top 1 μm of the nanowires than in their bottom 1 μm [Fig. 2(a)]. We tentatively attribute this finding to a larger donor concentration in the bottom segments, inducing radial electric fields of a magnitude sufficient to ionize excitons. In agreement with this interpretation, the transitions from the $(I_1,X)$ at 10 K and the free exciton at 300 K are observed only for the top segments of the nanowires. We emphasize that the intensities of the $(D^0,X)$ and $(I_1,X)$ transitions are not spatially anticorrelated [Fig. 2(d)]. A similar observation was made for layers with a BSF density on the order of $10^4$ cm$^{-1}$ [27], a density that would correspond to the presence of only a few BSFs per nanowire. The absence of a spatial anticorrelation between the $(I_1,X)$ and the $(D^0,X)$ lines arises from the fact that the characteristic times for the radiative decay of the FX and its capture by the BSFs are on the same order, in agreement with the results of Ref. [29]. We also do

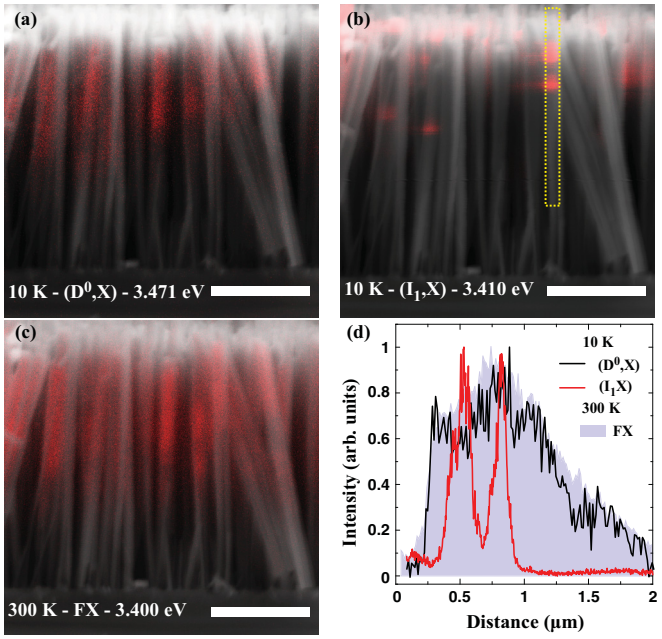


FIG. 2. (Color online) Superposition of scanning electron micrographs (gray scale) and monochromatic CL maps (false color) taken at 10 K at the emission energy of (a) the $(D^0,X)$ and (b) the $(I_1,X)$. The scale bar corresponds to 1 μm. (c) Same as (a) and (b) but taken at 300 K at the FX emission energy. (d) CL intensity of the $(D^0,X)$ and $(I_1,X)$ transitions at 10 K and of the FX line at 300 K along the nanowire highlighted by the yellow rectangle in (b).

not observe an anticorrelation between the intensities of the $(I_1,X)$ transition at 10 K and of the FX transition at 300 K [cf. Figs. 2(b)–2(d)]. Since the diffusion length in GaN is much shorter than the nanowire length [30,31], this observation indicates that BSFs in nanowires do not open an efficient nonradiative recombination channel. Note that the intensity of the FX band at 300 K follows that of the $(D^0,X)$ transition at 10 K [Fig. 2(d)], again suggesting that field ionization is the dominant mechanism determining the intensity of the radiative transitions in these nanowires.

With increasing temperature, the dissociation of the $(D^0,X)$ leads to the quenching of the corresponding transition to the benefit of the FX line (Fig. 1). Between 10 and 300 K, the FX transition redshifts, following a temperature dependence well described by the expression derived by Pässler [32] with the parameters recommended for GaN(0001) layers as shown in Fig. 3(a). In contrast to the FX transition, the energy of the $(I_1,X)$ band follows a half $S$-shaped temperature dependence: it blueshifts between 10 and 60 K and redshifts for larger $T$. This behavior reflects exciton localization along the BSF plane [25,27]. Since BSFs are free of strain and alloy disorder and exhibit abrupt interfaces, intra-BSF localization has been attributed previously to the presence of neutral donors in the vicinity of the BSF plane [9,27]. For $T > 60$ K, the $(I_1,X)$ and FX transitions redshift and exhibit an energy difference of $\Delta E = 54$ meV.

Figure 3(b) shows the temperature dependence of the PL intensities of the $(I_1,X)$ transition and of the sum of the intensities of the $(D^0,X)$ and FX transitions, obtained from a deconvolution of the spectra shown in Fig. 1. The

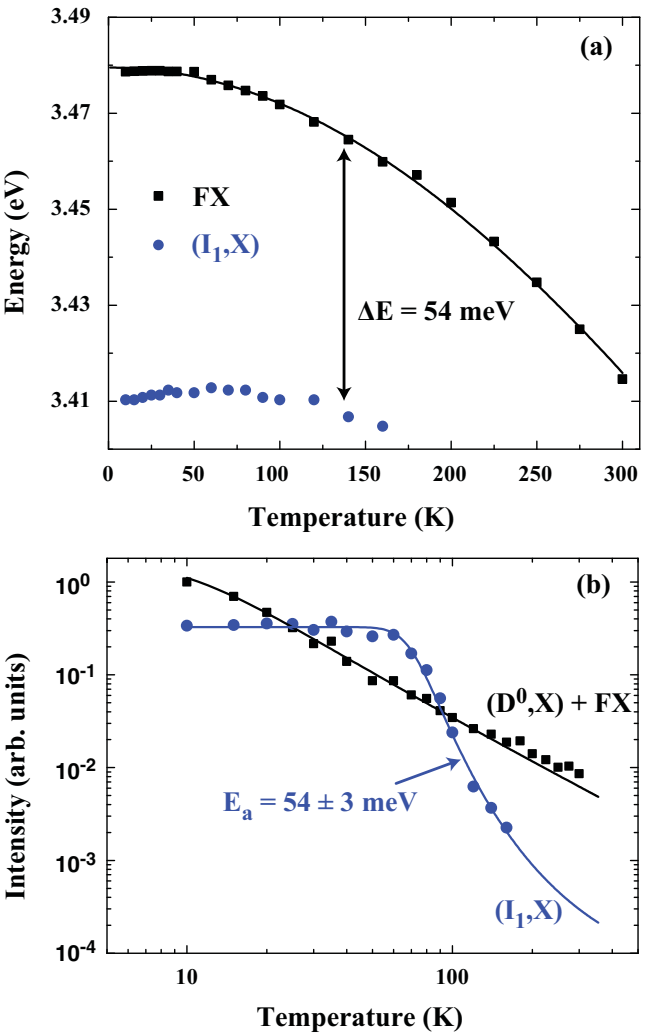


FIG. 3. (Color online) (a) FX (squares) and $(I_1,X)$ (circles) emission energies as a function of $T$. The solid line is a fit to the free exciton emission energy using the expression derived by Pässler [32]. $\Delta E = 54$ meV is the energy difference between the FX and the delocalized $(I_1,X)$. (b) Sum of the FX and $(D^0,X)$ emission intensities (squares) and $(I_1,X)$ emission intensity (circles) as a function of $T$, displayed on a double logarithmic scale. The black solid line is a fit to the total FX and $(D^0,X)$ intensity assuming that the nonradiative lifetime of FX is a constant and that its radiative lifetime increases with $T^{3/2}$. The blue solid line is the result of an Arrhenius fit to the $(I_1,X)$ emission intensity accounting for a nonradiative recombination channel with an activation energy $E_A = 54 \pm 3$ meV.

latter decreases following a $T^{-3/2}$ dependence, demonstrating (i) that the dynamics of the FX and the $(D^0,X)$ are dominated by nonradiative recombination already at cryogenic $T$, and (ii) that the decay rate of this nonradiative recombination channel is essentially constant over the whole temperature range since the radiative decay rate of the FX decreases with $T^{3/2}$ [33]. In contrast, the intensity of the $(I_1,X)$ transition remains constant between 10 and 60 K and quenches for larger $T$ following an Arrhenius behavior with an activation energy $E_a = 54 \pm 3$ meV. This value is equal to the energy difference $\Delta E$ determined from the data shown in Fig. 3(a), and we therefore attribute the quenching of the $(I_1,X)$ emission at

$T > 60$ K to the thermally activated detrapping of excitons as also found for GaN layers [25] and GaAs nanowires [9,34]. For nonpolar GaN layers [25], the delocalization of $(I_1,X)$ between 10 and 50 K is accompanied by the activation of a nonradiative recombination channel. This channel has been ascribed to the capture of $(I_1,X)$ by the nonradiative partial dislocations, which close the BSF plane [26,35]. Since BSFs in nanowires extend across the whole nanowire section [3,5], this additional nonradiative process is not observed in our sample [cf. Fig. 3(b)].

The constant $(I_1,X)$ emission intensity between 10 and 60 K may reflect two distinct scenarios. The first obvious explanation for this observation is that the $(I_1,X)$ decay is purely radiative over this temperature range. However, since the nonradiative lifetime of the FX and the $(D^0,X)$ is constant between 10 and 300 K, one could argue that it could also be constant for the $(I_1,X)$. Observing a constant $(I_1,X)$ emission intensity between 10 and 60 K would simply require the $(I_1,X)$ radiative lifetime to be constant as well, irrespective of the overall internal quantum efficiency of $(I_1,X)$. This second scenario would take place if the $(I_1,X)$ are localized between 10 and 60 K. The half *S*-shape dependence observed in Fig. 3(a) would then have to arise from the redistribution of excitons among these localized states. In the following, we carry out TR PL on our GaN nanowire ensemble focusing on the dynamics of the $(I_1,X)$ state to distinguish between the two scenarios discussed above.

### B. Density of states and oscillator strength of the stacking-fault exciton

PL transients recorded at 10 K of the FX, $(D^0,X)$, and $(I_1,X)$ transitions are shown in Fig. 4(a). While the FX emission intensity increases almost instantaneously, the $(D^0,X)$ emission intensity reaches its maximum after a delay of about 70 ps, which corresponds to the time required to capture excitons by neutral donors [22,36]. For longer time delays, the FX and $(D^0,X)$ transitions decay in parallel, indicating the thermalization of these two distributions of excitons [22,36]. The $(D^0,X)$ and FX transients are nearly exponential over the first 0.6 ns of the decay. They exhibit an effective exciton lifetime $\tau_{\text{eff}}^{\text{X}} = 190$ ps, which is given by

$$\frac{1}{\tau_{\text{eff}}^{\text{X}}} = \frac{1}{\tau_{\text{r}}} + \frac{1}{\tau_{\text{nr}}}, \tag{1}$$

where $\tau_{\text{r}}$ and $\tau_{\text{nr}}$ are the exciton radiative and nonradiative lifetimes, respectively. In high-quality GaN layers, $\tau_{\text{r}}$ for the $(D^0,X)$ state is at least 1 ns [37]. Therefore, the decay of the thermalized distribution of the FX and the $(D^0,X)$ in our GaN nanowires is certainly dominated by nonradiative phenomena [33]. After about 0.6 ns, the FX and $(D^0,X)$ transients deviate from a pure exponential behavior due to the coupling between these states and deeper states such as acceptor-bound excitons or the UX states [36].

Figure 4(a) shows that both the increase and the decay of the $(I_1,X)$ intensity are much slower than those measured for the $(D^0,X)$ intensity. First, the $(I_1,X)$ transition reaches its maximum intensity 125 ps after the $(D^0,X)$ line. The factor limiting the increase of the $(I_1,X)$ emission intensity is the transport of excitons from nanowire segments free of extended defects to the BSFs. This transport is inefficient as it takes place at low temperatures via the hopping of excitons from one donor to the next [29]. Second, the effective decay time for the $(I_1,X)$ recombination is $\tau_{\text{eff}}^{\text{BSF}} = 1.6$ ns, a decay time significantly longer than that reported so far for BSFs in group-III-nitride layers [27,29,38–41]. Moreover, this decay time is almost ten times longer than $\tau_{\text{eff}}^{\text{X}}$, which suggests that the $(I_1,X)$ are much less affected by nonradiative recombination than both the $(D^0,X)$ and FX.

In fact, Figs. 4(b) and 4(c) show that $\tau_{\text{eff}}^{\text{BSF}}$ increases from 1.6 to 5.6 ns between 10 and 60 K, and decreases subsequently to 0.7 ns when $T$ is increased further from 60 to 160 K. As detailed in Ref. [30], measuring simultaneously a constant emission intensity and an increase in $\tau_{\text{eff}}^{\text{BSF}}$ demonstrates the dominance of radiative phenomena over nonradiative ones. In other words, between 5 and 60 K, $\tau_{\text{r}}^{\text{BSF}} \approx \tau_{\text{eff}}^{\text{BSF}}$. For larger $T$, the thermal escape of charge carriers from the BSFs to the wurtzite matrix is activated [cf. Fig. 3(b)]. Considering that the density of states in the GaN wurtzite matrix is certainly

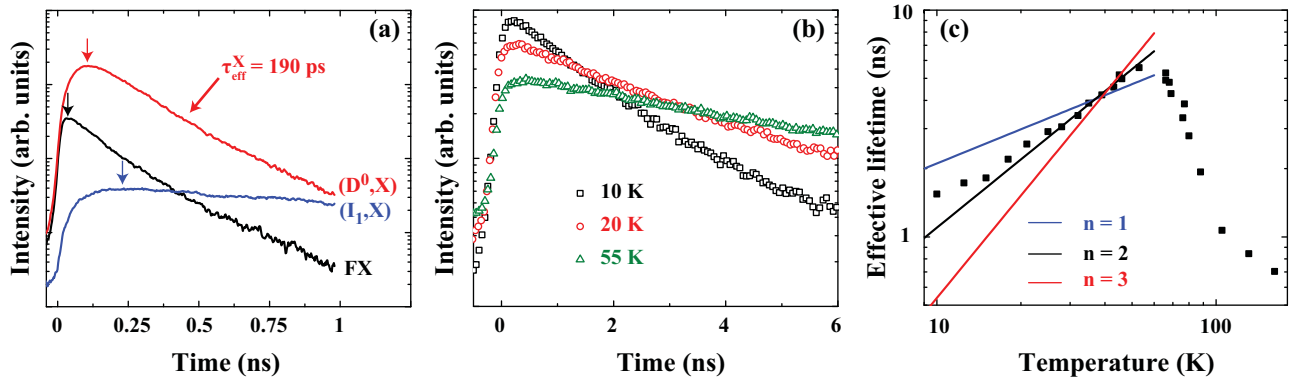


FIG. 4. (Color online) (a) PL intensity transients of the FX, $(D^0,X)$, and $(I_1,X)$ transitions at 10 K. The temporal resolution was set to 20 ps. The vertical arrows indicate the time at which each transient reaches its maximum intensity. The effective lifetime $\tau_{\text{eff}}^{\text{X}} = 190$ ps has been obtained from an exponential fit to the $(D^0,X)$ transient. (b) PL intensity transients of the $(I_1,X)$ transition at 10, 20, and 55 K. The temporal resolution was set to 160 ps. An exponential fit of these transients yields $\tau_{\text{eff}}^{\text{BSF}} = 1.6$, 2.9, and 5.6 ns for $T = 10$, 20, and 55 K, respectively. (c) Temperature dependence of $\tau_{\text{eff}}^{\text{BSF}}$ (squares). The solid lines show the result of the fits using Eq. (2) for $n = 1$ ($A = 0.666$ ns K$^{-1/2}$), $n = 2$ ($A = 0.110$ ns K$^{-1}$), and $n = 3$ ($A = 0.017$ ns K$^{-3/2}$).

much higher than in the BSFs, the dynamics of the $(I_1,X)$ is then governed by that of the FX [42]. Since the FX decay is mostly nonradiative already at 10 K, the thermal detrapping of excitons from BSFs for $T > 60$ K is accompanied by a rapid decrease in $\tau_{\mathrm{eff}}^{\mathrm{BSF}}$.

The ability to directly measure the increase of $\tau_{\mathrm{r}}^{\mathrm{BSF}}$ with $T$ facilitates the investigation of fundamental electronic properties of BSFs. The radiative lifetime $\tau_{\mathrm{r}}$ for a localized exciton is proportional to the exciton coherence volume and therefore does not vary with $T$ [43]. In contrast, the radiative lifetime of free excitons in the bulk (provided that the exciton scattering rates are faster than the exciton-photon coupling rate) or confined in a quantum well or quantum wire increases with $T$ [44–46]. This increase results from the fact that for higher $T$ excitons populate states that cannot couple to light. Using the results of Refs. [43–46], $\tau_r$ is given by

$$\tau_{\mathrm{r}} = AT^{n/2}, \tag{2}$$

where $0 \leqslant n \leqslant 3$ is the dimensionality of the system and $A$ is a constant. For $T > 20$ K, the increase in $\tau_{\mathrm{r}}^{\mathrm{BSF}}$ is linear $(n = 2)$, and we obtain $A = 0.11$ ns K$^{-1}$. Assuming $n = 1$ or $n = 3$ does not lead to an acceptable fit of the data [cf. Fig. 4(c)]. This finding shows conclusively that the density of states for free excitons confined to a BSF is two dimensional. Consequently, we experimentally confirm the proposal by Albrecht et al. [14] that a BSF forms a QW. We recall that we investigate here the emission properties of BSFs in nanowires with a mean diameter of 50 nm, which is about 15 times larger than the exciton Bohr radius [28]. When contained in planar heterostructures with the growth axis perpendicular to the BSF plane or in thinner nanowires, BSFs may lead to the formation of quantum structures with lower dimensionality such as quantum wires [47] or quantum dots [4].

The deviation of $\tau_{\mathrm{r}}^{\mathrm{BSF}}$ from a linear behavior for $T < 20$ K signifies the presence of localization centers in the vicinity of the BSF plane. Assuming that the $(I_1,X)$ relaxes to localization centers with a density $N_{\mathrm{D}}$ within a BSF faster than it decays, we obtain [30,48]

$$\tau_{\mathrm{r}}^{\mathrm{BSF}} = \frac{N_{\mathrm{loc}} + N_{\mathrm{fr}}}{N_{\mathrm{loc}}\Gamma_{\mathrm{loc}} + N_{\mathrm{fr}}\Gamma_{\mathrm{fr}}}, \tag{3}$$

where $N_{\mathrm{loc}}$ and $N_{\mathrm{fr}}$ are the densities of localized and free $(I_1,X)$ states, respectively, with decay rates $\Gamma_{\mathrm{loc}}$ and $\Gamma_{\mathrm{fr}}$, respectively. We assume that at 10 K all $(I_1,X)$ are localized and exhibit a radiative lifetime of $\tau_{\mathrm{loc}} = \Gamma_{\mathrm{loc}}^{-1} = 1.6$ ns [cf. Fig. 4(b)]. It follows directly from Eqs. (2) and (3) that $\tau_{\mathrm{r}}^{\mathrm{BSF}}$ is a constant for $N_{\mathrm{fr}} \ll N_{\mathrm{loc}}$, but a linear function of $T$ for $N_{\mathrm{fr}} \gg N_{\mathrm{loc}}$. Interestingly, the slope $A$ for the increase of $\tau_{\mathrm{r}}^{\mathrm{BSF}}$ with $T$ is affected by the presence of potential fluctations even when $N_{\mathrm{fr}} \gg N_{\mathrm{loc}}$. Specifically, $A$ is found to be inversely proportional to the density of localized states $N_{\mathrm{D}}$ for sufficiently high densities (see Appendix A for a derivation of this result):

$$A = 2\gamma k_B \left( f_{\mathrm{osc}} + \frac{\gamma \pi \hbar^2 N_{\mathrm{D}}}{M \tau_{\mathrm{loc}}} \right)^{-1}, \tag{4}$$

where $k_B$ is the Boltzmann constant, $f_{\mathrm{osc}}$ the oscillator strength of the free $(I_1,X)$, $N_{\mathrm{D}}$ the areal density of localized states in the BSF, and $M = 1.2m_0$ the exciton translational mass. The coefficient $\gamma$ is given by

$$\gamma = \frac{3m_0 c \epsilon_0 \sqrt{\epsilon}}{E_1 e^2}, \tag{5}$$

where $c$ is the speed of light in vacuum, $\epsilon = 9.5$ the relative permittivity of GaN, $e$ the elementary charge, and $E_1$ the exciton kinetic energy above which excitons cannot couple to light. In GaN, $E_1$ is on the order of 0.1 meV [30].

The value of $A$ measured for the $(I_1,X)$ state is much larger than for excitons in nonpolar (Al,Ga)N/GaN QWs, for which $A$ amounts to only a few ps K$^{-1}$ [42,49]. This result confirms that crystal-phase quantum structures exhibit improved interfaces and reduced densities of localization centers as compared to planar heterostructures. In addition we can estimate an upper limit for the oscillator strength $f_{\mathrm{osc}} < 1.5 \times 10^{12}$ cm$^{-2}$ for $N_{\mathrm{D}} \to 0$ [Eq. (4)]. This value is more than one order of magnitude smaller than the value expected for free excitons in (Al,Ga)N/GaN QWs free of electrostatic fields [30]. However, this low $f_{\mathrm{osc}}$ measured for the $(I_1,X)$ should not be taken as an evidence of a type-II band alignment between wurtzite and zinc-blende GaN. As shown in Ref. [8], the emission energy of the $(I_1,X)$ is insensitive to the band alignment. Analogously, within the frame of the model described in Ref. [28], we obtain a low $f_{\mathrm{osc}}$ regardless of the band alignment. In fact, the low oscillator strength of the $(I_1,X)$ is caused mainly by the presence of built-in electric fields that spatially separate the electron and hole wave functions also for a type-I band alignment. These fields arise from the discontinuity of the spontaneous polarization field at the interface between zinc-blende and wurtzite GaN and can exhibit a magnitude of a few MV/cm [8,50].

As shown in Appendix B, we have obtained similar values for $N_{\mathrm{D}}$, $f_{\mathrm{osc}}$, and $\tau_{\mathrm{eff}}^{\mathrm{BSF}}$ at 10 K for nanowire samples of very different diameter, coalescence degree, and BSF density. Our values differ from the results of Korona et al. [16], who have recently reported $\tau_{\mathrm{r}}^{\mathrm{BSF}} = 0.75$ ns at 10 K and $A = 0.015$ ns K$^{-1}$. However, while the BSFs in our nanowires are induced by a significant Si incorporation that lowers the BSF formation energy [21,51], the BSFs in Ref. [16] form upon the coalescence between adjacent nanowires. This coalescence between nanowires is additionally accompanied by the formation of a network of boundary dislocations [52], which are presumably nonradiative recombination centers. Therefore, the discrepancy between our results and those of Korona et al. [16] may stem from the presence of dislocations in the sample investigated in the latter work, inducing an additional nonradiative channel which in turn enhances the recombination rate at higher $T$. We also stress that the intentionally coalesced nanowire ensemble studied by Korona et al. [16] is expected to contain a very high density of BSFs [the intensity of the $(I_1,X)$ transition in the spectra shown in Ref. [16] is orders of magnitude higher than that of any other transition]. For samples with such a high density of BSFs, adjacent BSFs couple electronically [25], which may lead to a variation in $f_{\mathrm{osc}}$, $\tau_{\mathrm{r}}^{\mathrm{BSF}}$, and $A$ with respect to the values obtained here for nanowire ensembles with isolated BSFs [28].

The crossover between dominantly radiative and nonradiative recombination occurs at 60 K for the sample under

investigation. At this temperature, the nonradiative lifetime ($\tau_{nr}^{BSF}$) of the $(I_1,X)$ is necessarily larger than $\tau_{eff}^{BSF} \approx 6$ ns. At the same time, the $(I_1,X)$ is delocalized at this temperature and is free to diffuse along the BSF plane. Since the nanowire diameter $\phi$ is comparable to the diffusion length of the free exciton [31], the $(I_1,X)$ will probe the $M$-plane nanowire sidewall facets and recombine there nonradiatively via surface states if such states are present. If we assume that the quenching of the $(I_1,X)$ emission intensity arises exclusively from surface recombination, the surface recombination velocity is $S = \phi/(4\tau_{nr}^{BSF}) < 210$ cm s$^{-1}$, where $\phi = 50$ nm is the mean nanowire diameter. This value of $S$ is more than an order of magnitude smaller than what has been reported in Refs. [53,54] for GaN nanowires at 10 and 300 K, respectively. The surface recombination in GaN nanowires is thus either strongly temperature dependent, or the nonradiative recombination observed in Refs. [53,54] does not arise solely from the nanowire surface. However, since the nonradiative lifetime of the FX and the $(D^0,X)$ has been found to be almost constant between 10 and 300 K [33], the nanowire surface is most probably not the main nonradiative decay channel for excitons in our GaN nanowires.

## IV. SUMMARY AND CONCLUSIONS

Using time-resolved PL experiments on GaN nanowire ensembles, we have shown that the density of states of excitons bound to $I_1$ BSFs is two dimensional. This finding demonstrates that BSFs may indeed be considered as quantum wells. The recombination of the $(I_1,X)$ is purely radiative up to 60 K. The effective lifetime measured for the $(I_1,X)$ at 60 K indicates that the recombination velocity in our GaN nanowires is smaller than 210 cm s$^{-1}$. For larger $T$, the $(I_1,X)$ escape thermally from the BSFs and recombine nonradiatively, leading to a decrease in effective decay time for the $(I_1,X)$ recombination.

The fast decay of the FX and the $(D^0,X)$ at 10 K in GaN nanowires is dominated by a nonradiative channel that is most likely opened by point defects [33,55]. To explain the fast decay of the majority of $(D^0,X)$ states, the density of nonradiative centers has to be higher than $5 \times 10^{17}$ cm$^{-3}$ [55]. However, the FX and $(D^0,X)$ states were found to efficiently couple in GaN nanowires even at low temperatures [cf. Fig. 4(a)], and the $(D^0,X)$ may consequently decay *indirectly* via the FX [33]. In this case, it is not in general possible to ascertain whether it is the $(D^0,X)$ or the FX state which is actually affected by the nonradiative recombination [33].

Using the BSFs as a probe, we are able to distinguish between these two scenarios. A density of nonradiative centers of $5 \times 10^{17}$ cm$^{-3}$ is inconsistent with the observation of a dominantly radiative recombination in BSFs. As we probe several hundreds of BSFs in our experiments, the majority of them are required to be free of these nonradiative centers. Hence the density of these centers must be at least significantly lower than the inverse volume experienced by an $(I_1,X)$. Since the extent of the $(I_1,X)$ wave function along the nanowire axis amounts to about 8 nm [28] and the radial one is equal to the nanowire radius of 25 nm, the density of nonradiative centers *must* be well below $6 \times 10^{16}$ cm$^{-3}$. Evidently, this density is not compatible with the one required for the direct nonradiative decay of the $(D^0,X)$. If, however, the $(D^0,X)$ decays indirectly via the FX, even densities well below $1 \times 10^{16}$ cm$^{-3}$ are sufficient for opening an efficient nonradiative channel, since the diffusion length of the FX is reported to be larger than 50 nm [31].

## ACKNOWLEDGMENTS

The authors would like to thank Uwe Jahn for a critical reading of the manuscript and Henning Riechert for continuous encouragement and support. Partial financial support of this work by the Deutsche Forschungsgemeinschaft within SFB 951 is gratefully acknowledged.

## APPENDIX A: TEMPERATURE DEPENDENCE OF THE RADIATIVE LIFETIME OF THE STACKING-FAULT EXCITON

For evaluating the temperature ($T$) dependence of the radiative lifetime of excitons confined in an $I_1$ BSF in the presence of potential fluctuations, we follow the procedure established by Citrin [48]. The areal density of localized states in the BSF is denoted by $N_D$. The distributions of localized ($N_{loc}$) and free excitons ($N_{fr}$) with radiative decay rates $\Gamma_{loc}$ and $\Gamma_{fr}$, respectively, are supposed to be in thermal equilibrium. The radiative decay rate $\Gamma_r^{BSF}$ for the thermalized population of excitons confined to the BSF is then

$$\Gamma_r^{BSF} = \frac{N_{loc}\Gamma_{loc} + N_{fr}\Gamma_{fr}}{N_{loc} + N_{fr}}. \tag{A1}$$

When $T$ is high enough for $N_{loc} \ll N_{fr}$, we obtain

$$\tau_r^{BSF} = 1/\Gamma_r^{BSF} = \frac{1}{\Gamma_{fr}}\left(1 + \frac{N_{loc}\Gamma_{loc}}{N_{fr}\Gamma_{fr}}\right)^{-1}. \tag{A2}$$

If $N_{loc}$ and $N_{fr}$ follow Boltzmann distributions, the ratio between localized and free exciton densities is given by

$$\frac{N_{loc}}{N_{fr}} = \frac{N_D \pi \hbar^2}{2Mk_BT} \exp\left(\frac{E_{loc}}{k_BT}\right), \tag{A3}$$

where $M$ is the exciton translational mass and $E_{loc}$ is the exciton localization energy. While $\Gamma_{loc}$ is independent of $T$ [43], $\Gamma_{fr}$ decreases linearly with $T$ [45]:

$$\Gamma_{fr} = \frac{2E_1}{3k_BT}\frac{e^2 f_{osc}}{4\pi c m_0 n}, \tag{A4}$$

where $m_0$ is the electron mass, $c$ the velocity of light, $n$ the optical index, $e$ the elementary charge, $f_{osc}$ the oscillator strength of the free exciton, and $E_1$ the exciton kinetic energy above which free excitons are dark.

Combining Eqs. (A1)–(A4), the radiative lifetime of the exciton bound to the BSF becomes $\tau_r^{BSF} = AT$, where $A$ is given by Eq. (4).

## APPENDIX B: RADIATIVE LIFETIME OF THE STACKING-FAULT EXCITON WITH VARYING NANOWIRE MORPHOLOGY AND STACKING-FAULT DENSITY

This Appendix is intended to demonstrate that our conclusions are independent of the nanowire morphology and BSF

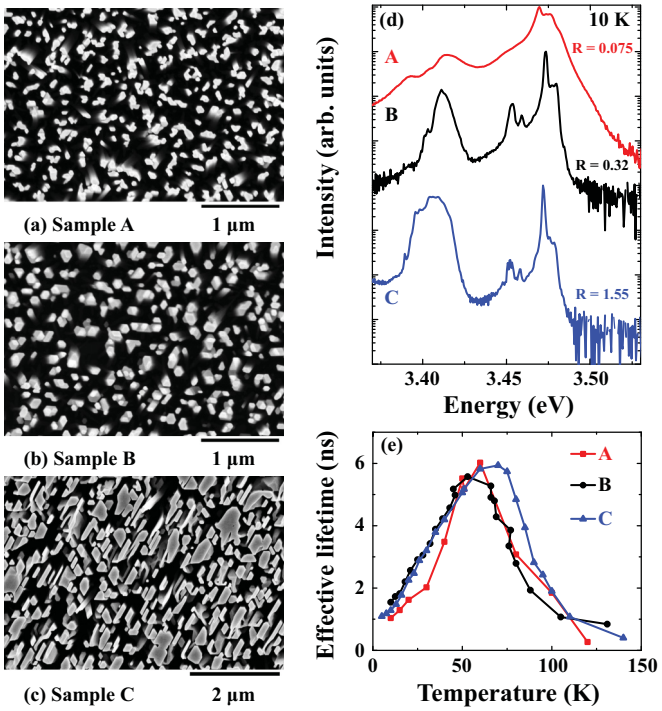


FIG. 5. (Color online) Top-view scanning electron micrographs of samples (a) A, (b) B, and (c) C. (d) PL spectra at 10 K for samples A, B, and C. The spectra are vertically shifted for clarity. $R$ is the ratio between the spectrally integrated intensities of the $(I_1,X)$ transition and the sum of the $(D^0,X)$ and FX transitions. (e) Decay time of the $(I_1,X)$ band as a function of $T$ for samples A, B, and C.

density. Figures 5(a)–5(c) show top-view scanning electron micrographs of samples A, B, and C which were grown at substrate temperatures of 835, 875, and 905 °C, respectively (sample B is the nanowire ensemble sample studied in the main text). Sample A has the smallest average diameter and coalescence degree. Sample C has an unusual, anisotropic morphology due to the fact that it was not rotated during growth. At the same time, the dimensions of the nanostructures in Fig. 5(c) are clearly larger than those of the nanowires in sample B.

Figure 5(d) displays the low-temperature (10 K) PL spectra of these three nanowire ensembles. With increasing growth temperature, the donor-bound exciton line becomes narrower: the $(D^0,X)$ transition has a linewidth of 1 meV for sample A, but 0.6 meV for samples B and C. Simultaneously, the higher the growth temperature, the stronger is the band related to the $I_1$ basal-plane stacking faults (BSF). The figure also shows the ratio $R$ between the integrated intensities of the $(I_1,X)$ and the sum of the $(D^0,X)$ and FX transitions. This ratio increases by a factor of 20 between samples A and C.

Figure 5(e) shows the decay times measured for samples A to C at temperatures between 10 and 140 K. Despite the different growth conditions and the resulting different morphologies and BSF densities, all samples exhibit a very similar dependence of the decay time with temperature. In particular, all samples are characterized by purely radiative recombination between 10 and 60 K and a similar slope for the increase of $\tau_r^{BSF}$ with temperature. The conclusions drawn from these experiments would thus be the same, regardless of the sample.


[1] F. Glas, J.-C. Harmand, and G. Patriarche, Phys. Rev. Lett. **99**, 146101 (2007).

[2] P. Caroff, K. A. Dick, J. Johansson, and M. E. Messing, Nat. Nanotechnol. **4**, 50 (2008).

[3] R. E. Algra, M. A. Verheijen, M. T. Borgström, L.-F. Feiner, G. Immink, W. J. P. van Enckevort, E. Vlieg, and E. P. A. M. Bakkers, Nature (London) **456**, 369 (2008).

[4] N. Akopian, G. Patriarche, L. Liu, J.-C. Harmand, and V. Zwiller, Nano Lett. **10**, 1198 (2010).

[5] P. Corfdir, B. Van Hattem, E. Uccelli, S. Conesa-Boj, P. Lefebvre, A. Fontcuberta i Morral, and R. T. Phillips, Nano Lett. **13**, 5303 (2013).

[6] J. Bolinsson, P. Caroff, B. Mandl, and K. A. Dick, Nanotechnology **22**, 265606 (2011).

[7] G. Jacopin, L. Rigutti, L. Largeau, F. Fortuna, F. Furtmayr, F. H. Julien, M. Eickhoff, and M. Tchernycheva, J. Appl. Phys. **110**, 064313 (2011).

[8] J. Lähnemann, O. Brandt, U. Jahn, C. Pfüller, C. Roder, P. Dogan, F. Grosse, A. Belabbes, F. Bechstedt, A. Trampert, and L. Geelhaar, Phys. Rev. B **86**, 081302 (2012).

[9] A. M. Graham, P. Corfdir, M. Heiss, S. Conesa-Boj, E. Uccelli, A. Fontcuberta i Morral, and R. T. Phillips, Phys. Rev. B **87**, 125304 (2013).

[10] S. Castelletto, Z. Bodrog, A. P. Magyar, A. Gentle, A. Gali, and I. Aharonovich, Nanoscale **6**, 10027 (2014).

[11] T. Kouno, M. Sakai, K. Kishino, and K. Hara, Jpn. J. Appl. Phys. **53**, 068001 (2014).

[12] T. T. T. Vu, T. Zehender, M. A. Verheijen, S. R. Plissard, G. W. G. Immink, J. E. M. Haverkort, and E. P. A. M. Bakkers, Nanotechnology **24**, 115705 (2013).

[13] L. Ahtapodov, J. Todorovic, P. Olk, T. Mjåland, P. Slåttnes, D. L. Dheeraj, A. T. J. Helvoort, B.-O. Fimland, and H. Weman, Nano Lett. **12**, 6090 (2012).

[14] M. Albrecht, S. Christiansen, G. Salviati, C. Zanotti-Fregonara, Y. T. Rebane, Y. G. Shreter, M. Mayer, A. Pelzmann, M. Kamp, K. J. Ebeling, M. D. Bremser, R. F. Davis, and H. P. Strunk, MRS Symp. Proc. **468**, 293 (1997).

[15] C. Stampfl and C. G. Van de Walle, Phys. Rev. B **57**, R15052 (1998).

[16] K. Korona, A. Reszka, M. Sobanska, P. Perkowska, A. Wysmolek, K. Klosek, and Z. Zytkiewicz, J. Lumin. **155**, 293 (2014).

[17] S. Fernández-Garrido, J. Grandal, E. Calleja, M. A. Sánchez-García, and D. Lopez-Romero, J. Appl. Phys. **106**, 126102 (2009).

[18] L. Geelhaar, C. Chèze, B. Jenichen, O. Brandt, C. Pfüller, S. Münch, R. Rothemund, S. Reitzenstein, A. Forchel, T. Kehagias, P. Komninou, G. P. Dimitrakopulos, T. Karakostas, L. Lari, P. R. Chalker, M. H. Gass, and H. Riechert, IEEE J. Sel. Top. Quantum Electron. **17**, 878 (2011).

[19] V. Consonni, Phys. Status Solidi RRL **7**, 699 (2013).
[20] B. Heying, R. Averbeck, L. F. Chen, E. Haus, H. Riechert, and J. S. Speck, J. Appl. Phys. **88**, 1855 (2000).
[21] P. Corfdir, J. K. Zettler, C. Hauswald, S. Fernández-Garrido, O. Brandt, and P. Lefebvre, Phys. Rev. B **90**, 205301 (2014).
[22] P. Corfdir, P. Lefebvre, J. Ristić, P. Valvin, E. Calleja, A. Trampert, J.-D. Ganière, and B. Deveaud-Plédran, J. Appl. Phys. **105**, 013113 (2009).
[23] E. Calleja, M. A. Sánchez-García, F. J. Sánchez, F. Calle, F. B. Naranjo, E. Muñoz, U. Jahn, and K. Ploog, Phys. Rev. B **62**, 16826 (2000).
[24] P. Lefebvre, S. Fernández-Garrido, J. Grandal, J. Ristić, M.-A. Sánchez-García, and E. Calleja, Appl. Phys. Lett. **98**, 083104 (2011).
[25] P. P. Paskov, R. Schifano, B. Monemar, T. Paskova, S. Figge, and D. Hommel, J. Appl. Phys. **98**, 093519 (2005).
[26] T. Gühne, Z. Bougrioua, S. Laügt, M. Nemoz, P. Vennéguès, B. Vinter, and M. Leroux, Phys. Rev. B **77**, 075308 (2008).
[27] P. Corfdir, P. Lefebvre, J. Levrat, A. Dussaigne, J.-D. Ganière, D. Martin, J. Ristić, T. Zhu, N. Grandjean, and B. Deveaud-Plédran, J. Appl. Phys. **105**, 043102 (2009).
[28] P. Corfdir and P. Lefebvre, J. Appl. Phys. **112**, 053512 (2012).
[29] P. Corfdir, J. Ristić, P. Lefebvre, T. Zhu, D. Martin, A. Dussaigne, J. D. Ganière, N. Grandjean, and B. Deveaud-Plédran, Appl. Phys. Lett. **94**, 201115 (2009).
[30] P. Corfdir, J. Levrat, A. Dussaigne, P. Lefebvre, H. Teisseyre, I. Grzegory, T. Suski, J.-D. Ganière, N. Grandjean, and B. Deveaud-Plédran, Phys. Rev. B **83**, 245326 (2011).
[31] G. Nogues, T. Auzelle, M. Den Hertog, B. Gayral, and B. Daudin, Appl. Phys. Lett. **104**, 102102 (2014).
[32] R. Pässler, J. Appl. Phys. **90**, 3956 (2001).
[33] C. Hauswald, P. Corfdir, J. K. Zettler, V. M. Kaganer, K. K. Sabelfeld, S. Fernández-Garrido, T. Flissikowski, V. Consonni, T. Gotschke, H. T. Grahn, L. Geelhaar, and O. Brandt, Phys. Rev. B **90**, 165304 (2014).
[34] D. Rudolph, L. Schweickert, S. Morkötter, L. Hanschke, S. Hertenberger, M. Bichler, G. Koblmüller, G. Abstreiter, and J. J. Finley, New J. Phys. **15**, 113032 (2013).
[35] Z. H. Wu, A. M. Fischer, F. A. Ponce, B. Bastek, J. Christen, T. Wernicke, M. Weyers, and M. Kneissl, Appl. Phys. Lett. **92**, 171904 (2008).
[36] C. Hauswald, T. Flissikowski, T. Gotschke, R. Calarco, L. Geelhaar, H. T. Grahn, and O. Brandt, Phys. Rev. B **88**, 075312 (2013).
[37] B. Monemar, P. P. Paskov, J. P. Bergman, G. Pozina, A. A. Toropov, T. V. Shubina, T. Malinauskas, and A. Usui, Phys. Rev. B **82**, 235202 (2010).
[38] L. Lahourcade, J. Renard, B. Gayral, E. Monroy, M. P. Chauvat, and P. Ruterana, J. Appl. Phys. **103**, 093514 (2008).
[39] T. J. Badcock, M. J. Kappers, M. A. Moram, P. Dawson, and C. J. Humphreys, Phys. Status Solidi B **249**, 498 (2012).
[40] M. Kagaya, P. Corfdir, J.-D. Ganière, B. Deveaud-Plédran, N. Grandjean, and S. F. Chichibu, Jpn. J. Appl. Phys. **50**, 111002 (2011).
[41] K. Furusawa, Y. Ishikawa, M. Tashiro, K. Hazu, S. Nagao, H. Ikeda, K. Fujito, and S. F. Chichibu, Appl. Phys. Lett. **103**, 052108 (2013).
[42] P. Corfdir, A. Dussaigne, H. Teisseyre, T. Suski, I. Grzegory, P. Lefebvre, E. Giraud, J.-D. Ganière, N. Grandjean, and B. Deveaud-Plédran, J. Appl. Phys. **111**, 033517 (2012).
[43] E. I. Rashba and G. E. Gurgenishvili, Sov. Phys. Solid State **4**, 759 (1962).
[44] G. W. 't Hooft, W. A. J. A. van der Poel, L. W. Molenkamp, and C. T. Foxon, Phys. Rev. B **35**, 8281 (1987).
[45] L. C. Andreani, F. Tassone, and F. Bassani, Solid State Commun. **77**, 641 (1991).
[46] D. S. Citrin, Phys. Rev. Lett. **69**, 3393 (1992).
[47] A. Dussaigne, P. Corfdir, J. Levrat, T. Zhu, D. Martin, P. Lefebvre, J.-D. Ganière, R. Butté, B. Deveaud-Plédran, N. Grandjean, Y. Arroyo, and P. Stadelmann, Semicond. Sci. Technol. **26**, 025012 (2011).
[48] D. S. Citrin, Phys. Rev. B **47**, 3832 (1993).
[49] D. Rosales, B. Gil, T. Bretagnon, B. Guizal, F. Zhang, S. Okur, M. Monavarian, N. Izyumskaya, V. Avrutin, U. Ozgur, H. Morkoç, and J. H. Leach, J. Appl. Phys. **115**, 073510 (2014).
[50] Y. J. Sun, O. Brandt, U. Jahn, T. Y. Liu, A. Trampert, S. Cronenberg, S. Dhar, and K. H. Ploog, J. Appl. Phys. **92**, 5714 (2002).
[51] J. A. Chisholm and P. D. Bristowe, Appl. Phys. Lett. **77**, 534 (2000).
[52] V. Consonni, M. Knelangen, U. Jahn, A. Trampert, L. Geelhaar, and H. Riechert, Appl. Phys. Lett. **95**, 241910 (2009).
[53] A. Gorgis, T. Flissikowski, O. Brandt, C. Chèze, L. Geelhaar, H. Riechert, and H. T. Grahn, Phys. Rev. B **86**, 041302(R) (2012).
[54] J. B. Schlager, K. A. Bertness, P. T. Blanchard, L. H. Robins, A. Roshko, and N. A. Sanford, J. Appl. Phys. **103**, 124309 (2008).
[55] C. Hauswald, T. Flissikowski, H. T. Grahn, L. Geelhaar, H. Riechert, and O. Brandt, Proc. SPIE **8986**, 89860V (2014).